18TH WORLD CONFERENCE ON EARTHQUAKE ENGINEERING
WCEE2024
MILAN

MILAN, ITALY
30TH JUNE - 5TH JULY 2024
www.wcee2024.it

LOCALLY RESONANT METAMATERIALS FOR CONTROLLING SEISMIC LOVE WAVES

F. Zeighami[1], A. Palermo[1] & A. Marzani[1]

[1] Department of Civil, Chemical, Environmental, and Materials Engineering (DICAM), University of Bologna, Bologna, Italy. farhad.zeighami3@unibo.it, antonio.palermo6@unibo.it, alessandro.marzani@unibo.it.

Abstract: In this work, we discuss the possibility of designing a resonant layer to effectively attenuate the propagation of seismic Love waves. To do so, we consider a medium comprising a resonant layer of arbitrary thickness made of locally resonant metamaterials placed over an isotropic and homogeneous half-space. The resonant layer is made of several rows of mechanical resonators embedded within the soil medium. Each row includes an array of periodically distributed resonators with dimensions much smaller than the wavelength of Love waves in the frequency range of interest. We exploit a homogenization technique to estimate the effective parameters of the resonant layer, which are valid in the long-wavelength regime. We then derive the dispersion law of Love waves traveling within the homogenized equivalent resonant layer. The dynamic interaction between the Love waves and the resonant layer yields a low-frequency bandgap stemming from the local resonance mechanism of the embedded resonators. Within this specific frequency range, the propagation of Love waves is prevented. Furthermore, we design meter-size resonators based on the derived dispersion relation to attenuate the propagation of Love waves in the frequency range relevant to ground-borne vibration isolation applications. Finally, we perform a parametric study to investigate the effect of the design parameters of the resonators on the extension of the bandgap frequency range.

1. Introduction

Elastic metamaterials are engineered composite materials with extraordinary mechanical properties different from those typically found in natural materials, including, for example, negative mass density and negative Poisson's ratio (Jiao, Mueller et al. 2023). The emergence of elastic metamaterials has constituted a significant advancement in material science. These materials have found diverse applications in the past two decades, among others, in civil engineering, including earthquake engineering. Within this context, the use of seismic metamaterials, a subset of elastic metamaterials, has developed as an innovative technique for protecting vulnerable and critical structures and infrastructure from earthquake damage (Brûlé, Javelaud et al. 2014, Krodel, Thome et al. 2015, Colombi, Roux et al. 2016, Miniaci, Krushynska et al. 2016, Pu and Shi 2018, Pu, Palermo et al. 2020).

Seismic metamaterials can be categorized based on their bandgap formation mechanisms (Mu, Shu et al. 2020), encompassing Bragg scattering (Brûlé, Javelaud et al. 2014), local resonance (Colombi, Roux et al. 2016, Palermo, Krödel et al. 2016), inertial amplification (Zeighami, Palermo et al. 2019), and transform mechanisms (Brûlé, Ungureanu et al. 2017). Over the past decade, different wave barriers have been proposed and developed employing these mechanisms. Among all these metamaterial-based barriers, locally resonant wave barriers, also referred to as seismic metasurfaces, provide wave-impeding devices with smaller dimensions that are not correlated to the wavelength of incident seismic waves (Palermo, Krödel et al. 2016, Colquitt, Colombi et al. 2017). Seismic metasurfaces operate based on local resonance. They have resonant frequencies tuned to the low-frequency range, typically below 10 Hz, relevant to seismic action. One of their

distinctive advantages is their installation along the path of seismic wave propagation which eliminates the necessity for construction alterations to the target structure.

Seismic metasurfaces are passive isolation systems that are activated by the motion of incoming seismic waves. These metasurfaces consist of an array of surface resonant structures, such as resonators or pillars, placed near the soil surface in close proximity to the target structures (Colombi, Ageeva et al. 2017, Pillarisetti, Lissenden et al. 2022, Zeighami, Sandoval et al. 2023). In the case of seismic Rayleigh waves propagating along an isotropic and homogeneous half-space equipped with an array of surface resonators, this dynamic interaction results in the generation of a low-frequency bandgap (BG), within which Rayleigh waves cannot propagate (Palermo, Krödel et al. 2016, Colquitt, Colombi et al. 2017). The ability of metasurfaces to attenuate Rayleigh waves has been confirmed through small-scale experiments (Palermo, Krödel et al. 2016, Zaccherini, Palermo et al. 2020).

Recent advancements in the field of locally resonant metamaterials field have given rise to resonant wave barriers that incorporate thick resonant layers to facilitate the attenuation of surface Rayleigh waves by introducing wider bandgaps within their frequency spectrum (Zeighami, Palermo et al. 2021). These resonant layers are constructed by arranging multiple layers of resonators embedded within a host medium (e.g., soil surface layer for the case of seismic barriers), with each resonator connected to the host medium via elastic links. In this configuration, the bandgap frequency range can be broadened by increasing the depth of the resonant layer, providing flexibility in controlling surface waves across various wavelength scales. In the case of seismic Love waves, their interaction with elastic metasurfaces results in the hybridization of the fundamental Love mode without forming a bandgap (Maurel, Marigo et al. 2018, Palermo and Marzani 2018, Xu, Cao et al. 2023). Exploiting modifications in the phase velocity of the fundamental Love mode, gradient-index lenses have been designed to redirect the propagation of Love waves (Palermo and Marzani 2018).

In our current research, we explore the possibility of designing a thick resonant layer to attenuate the transmission of seismic Love waves. This involves considering a layered medium, encompassing a resonant layer of arbitrary thickness consisting of locally resonant metamaterials positioned atop an isotropic and homogeneous half-space. The resonant layer is equipped with several rows of horizontally oriented resonators embedded within the soil medium, characterized by dimensions considerably smaller than the wavelength of Love waves at the target frequency. Our approach relies on homogenization techniques to estimate the effective parameters that govern the dynamic behavior of the resonant layer. These parameters are essential in deriving the dispersion law that characterizes Love wave propagation through the equivalent homogenized model of the resonant layer. Using the dispersion law, we explore the feasibility of introducing a bandgap within the frequency spectrum of seismic Love waves and analyze the factors that influence its formation. Ultimately, we provide practical guidelines for designing resonators of meter-scale dimensions, informed by the derived dispersion relation, to effectively manipulate the propagation of Love waves within the frequency range relevant to seismic isolation applications.

The paper is structured as follows: Section 2 provides the analytical derivation of the dispersion relation. In Section 3, we describe the numerical design of a thick locally resonant barrier specifically tailored for seismic Love waves by showing the results of the dispersion relations, accompanied by a parametric analysis of the resonator design parameters. Finally, Section 4 discusses our research conclusions.

2. Dispersion law for Love waves coupled with thick locally resonant metamaterials

We investigate the propagation of seismic Love waves through a resonant layer comprised of embedded resonators attached to a non-resonant half-space, as shown in Figure 1a. The resonant layer is composed of mechanical oscillators distributed randomly within a host material (referred to as "layer 1"). This hosting media has a finite depth, denoted as H, with mass density (ρ_1) and shear wave velocity (β_1). Each individual resonator consists of a rigid mass (m_r) suspended by horizontal and vertical springs with identical axial stiffness $K_{r,x} = K_{r,y} = K$ (as shown in the inset of Figure 1). This setup leads to the existence of degenerate resonant modes characterized by an angular frequency $\omega_{r,x} = \omega_{r,y} = \omega_r = 2\pi f_r = \sqrt{K/m_r}$ along the $x-y$ axes, where f_r is the resonant frequency in Hz. The dimensions of embedded resonators are intentionally chosen to ensure that their interaction with Love waves occurs at the subwavelength scale. The stiffer half-space (referred to as "layer 2") is isotropic, homogeneous, and elastic, characterized by mechanical parameters ρ_2 and β_2, with β_2

being greater than β_1. The shear modulus of the layers is represented as $\mu_j = \rho_j \beta_j^2$, where $j = 1,2$ corresponds to the soft layer and half-space, respectively.

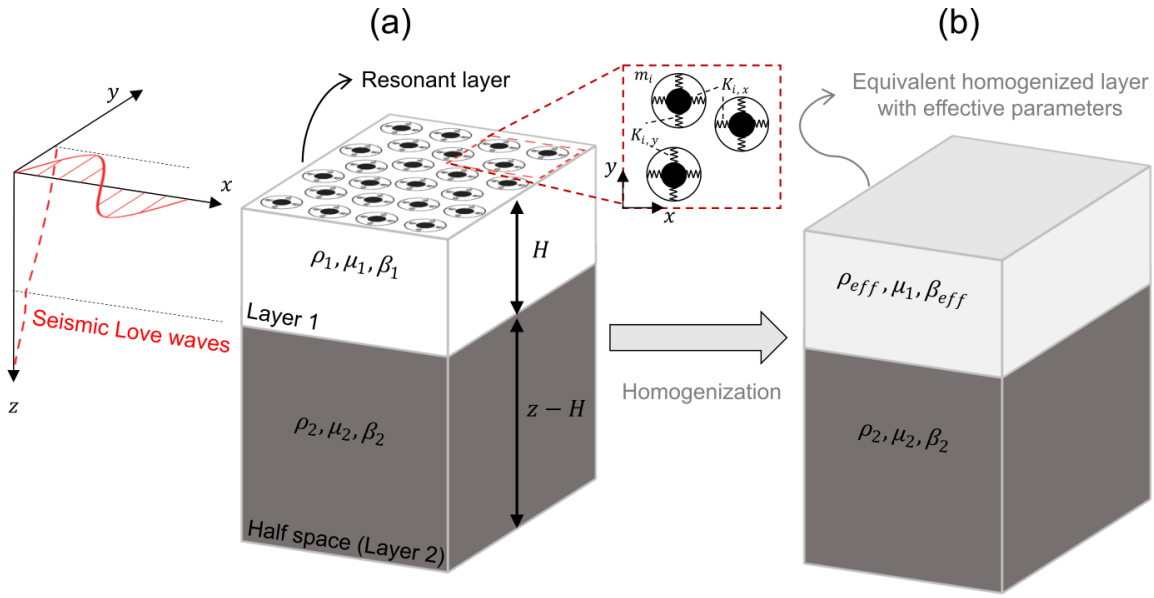

Figure 1. Schematic of seismic Love waves interacting with (a) an array of embedded locally resonant inclusions and (b) equivalent effective layer over rigid homogeneous half-space.

3.1. Effective parameters of locally resonant metamaterials

We introduce a Cartesian coordinate system as *x*-*y*-*z* and consider a harmonic Love wave with an angular frequency ω, wave phase velocity c, and wavenumber $k = \omega/c$, propagating along the *x*-direction and polarized along the *y*-direction. In what follows, we will characterize the dispersive properties of horizontally polarized surface waves within a finite-depth resonant layer coupled to a stiffer non-resonant half-space.

By virtue of the above-mentioned assumptions, the dynamics of the embedded mechanical resonators can be effectively described through the concept of an "equivalent homogenous layer," as visualized in Figure 1b. This approach enables us to model the resonant layer as an equivalent homogeneous layer characterized by frequency-dependent mass density and bulk wave velocity. We remark that our estimation of the effective mechanical parameters for this homogenized layer is tailored to the long-wavelength approximation, ensuring its applicability in the context of our analysis.

To derive these effective mechanical parameters, we assume that the resonant layer consists of n_r discrete resonators embedded within the soft layer, having a reference volume of $V = A \times H$, where $A = L^2$ represents the surface area, and H is the depth of the host medium (in this case, "layer 1"). As a result, the resonant layer can be modeled as a homogenous medium (Huang, Sun et al. 2009), having a frequency-dependent effective mass density of:

$$\rho_{eff}(\omega) = \frac{m_1 + n_r m_r}{V} + \frac{n_r m_r}{V} \frac{\omega^2}{{\omega_r}^2 - \omega^2} = \rho_1 \left(1 + \alpha \left(1 + \frac{\omega^2}{{\omega_r}^2 - \omega^2}\right)\right), \qquad (1)$$

where m_1 represents the mass of host material (layer 1) enclosed within the reference volume, m_r denotes the mass of resonators, and $\alpha = \rho_r/\rho_1$ is the ratio between the resonator mass per unit volume and the mass density of the host layer. We note that for $\omega_r \to \infty$ the effective mass density becomes equivalent to the static mass density, which we denote as $\rho_{st} = m_1 + n_r m_r/V = \rho_1 + \rho_r$, and this holds true for all frequency values. Conversely, where the existence of resonators is discarded ($\omega_r = 0$), the effective mass density becomes equal to the mass density of layer 1 ($\rho_{eff}(\omega) = \rho_1$).

Given our interest in the low-frequency response of the local resonators, the mechanical properties of the homogenized composite material can be estimated following the calculation of its effective shear wave velocity as follows:

$$\beta_{eff}(\omega) = \sqrt{\frac{\mu_1}{\rho_{eff}(\omega)}} = \sqrt{\frac{\mu_1}{\rho_1\left(1+\alpha\left(1+\frac{\omega^2}{{\omega_r}^2-\omega^2}\right)\right)}}. \quad (2)$$

3.2. 2.2 Analytical derivation of dispersion relation

Having derived the effective parameters for the equivalent homogenized resonant layer, we now study the propagation of horizontally polarized surface waves in this homogenized layer having depth of H placed over a semi-infinite non-resonant medium, as shown in Figure 1b. The mechanical properties of the homogenized layer are described by exploiting its frequency-dependent effective properties, namely $\rho_{eff}(\omega)$ and $\beta_{eff}(\omega)$, whereas the isotropic, homogeneous half-space is characterized by mass density denoted as ρ_2 and shear wave velocity β_2.

Let us consider a Love wave propagating in the $x-y$ plane, the displacement vectors in the homogenized resonant layer $\boldsymbol{u}_1$ and the half-space $\boldsymbol{u}_2$ for $z>0$ read:

$$\boldsymbol{u}_j = [u_j, v_j, w_j],\ j = 1,2, \quad (3)$$

where $u_1 = u_2 = w_1 = w_2 = 0$ are null displacement components for shear-horizontal waves. As such, the only non-zero displacement component of the resonant layer and half-space is:

$$v_1(x,z,t) = f(z)e^{i(\omega t - kx)},\quad v_2(x,z,t) = g(z)e^{i(\omega t-kx)}. \quad (4)$$

The equation of motion for the shear bulk waves reads:

$$\nabla^2 v_j = \frac{1}{(\beta_j)^2}\frac{\partial^2 v_j}{\partial t^2},\ j = 1,2, \quad (5)$$

which can be written for the resonant layer and non-resonant half-space in the forms of:

$$\nabla^2 v_1 = \frac{1}{(\beta_{eff}(\omega))^2}\frac{\partial^2 v_1}{\partial t^2},\ \nabla^2 v_2 = \frac{1}{(\beta_2)^2}\frac{\partial^2 v_2}{\partial t^2}. \quad (6)$$

From Eq. (6), two ordinary differential equations (ODEs) are derived as:

$$f''(z) + \frac{\omega^2}{c^2}\left(\frac{c^2}{\beta_{eff}(\omega)^2}-1\right)f(z) = 0,\ g''(z) + \frac{\omega^2}{c^2}\left(\frac{c^2}{{\beta_2}^2}-1\right)g(z) = 0. \quad (7)$$

The general solutions of ODEs of Eq. (7) are:

$$f(z) = A_1 e^{iks_1 z} + A_2 e^{-iks_1 z},\ g(z) = A_3 e^{iks_2 z} + A_4 e^{-iks_2 z}, \quad (8)$$

where $A_1, \dots, A_4$ are four unknown wave amplitudes and s_j is given for $j = 1,2$, as:

$$s_1(\omega) = \sqrt{\left(\frac{c}{\beta_{eff}(\omega)}\right)^2 - 1},\quad s_2 = \sqrt{\left(\frac{c}{\beta_2}\right)^2 - 1}. \quad (9)$$

The displacement components of Eq. (4) can be updated as:

$$\begin{aligned} v_1(x,z,t) &= \left(A_1 e^{iks_1(\omega)z} + A_2 e^{-iks_1(\omega)z}\right)e^{i(\omega t-kx)},\\ v_2(x,z,t) &= \left(A_3 e^{-iks_2{}^* z} + A_4 e^{-iks_2 z}\right)e^{i(\omega t-kx)}, \end{aligned} \quad (10)$$

in which,

$$s_2 = i\,s_2{}^*,\quad s_2{}^* = \sqrt{1-\left(\frac{c}{\beta_2}\right)^2}. \quad (11)$$

The classical dispersion relation derivation of Love waves (Love 1911) adopts the following set of boundary conditions to determine the four arbitrary unknown constants, $A_1, \dots, A_4$ in Eq. (10), as:

$$\tau_{zy,1} = \mu_1 \frac{\partial v_1}{\partial z} = 0, \text{ for } z = 0, \tag{12}$$

$$v_1 = v_2, \text{ for } z = H, \tag{13}$$

$$\tau_{zy,1} = \tau_{zy,2} \Leftrightarrow \mu_1 \frac{\partial v_1}{\partial z} = \mu_2 \frac{\partial v_2}{\partial z}, \text{ for } z = H, \tag{14}$$

$$v_2(z) \to 0, \text{ for } z \to \infty, \tag{15}$$

namely, null tangential stress at the free surface boundary (Eq. (12)), null displacement at infinite depth (Eq. (15)), and continuity of displacements and tangential stresses at the interface between the resonant layer and non-resonant half-space, Eq. (13), and Eq. (14), respectively.

After dropping the common propagating term ($e^{i(\omega t - kx)}$) and substituting the expressions $A_1 = A_2$ obtained from Eq. (12) and $A_4 = 0$ obtained from Eq. (15), the boundary value problem is reduced to a system of two independent equations. These equations refer to the continuity of displacements and tangential stresses at the interface, and they can be rearranged in a matrix form as

$$\begin{bmatrix} 2\cos(ks_1(\omega)H) & -e^{-ks_2{}^*H} \\ -2\mu_1 ks_1(\omega)\sin(ks_1(\omega)H) & \mu_2 ks_2{}^* e^{-ks_2{}^*H} \end{bmatrix} \begin{bmatrix} A_1 \\ A_3 \end{bmatrix} = \begin{bmatrix} 0 \\ 0 \end{bmatrix}, \tag{16}$$

or can be written in a compact form as $\boldsymbol{D}(k,\omega)\boldsymbol{A} = \boldsymbol{0}$. The non-trivial solutions of Eq. (16) in terms of variables ω and k provide the dispersion law of Love waves propagating in a resonant layer attached to a rigid half-space. These solutions are obtained by imposing the $\det\big(\boldsymbol{D}(k,\omega)\big) = 0$ as:

$$\tan(ks_1(\omega)H) = \frac{\mu_2 s_2{}^*}{\mu_1 s_1(\omega)}, \tag{17}$$

or equivalently

$$kH\sqrt{\left(\frac{\omega}{k\beta_{eff}(\omega)}\right)^2 - 1} = \arctan\left(\frac{\sqrt{1-\left(\frac{\omega}{k\beta_2}\right)^2}}{\mu^*\sqrt{\left(\frac{\omega}{k\beta_{eff}(\omega)}\right)^2 - 1}}\right) + n\pi, \tag{18}$$

where n is an integer indicating the surface Love mode number and $\mu^* = \mu_1/\mu_2$ the ratio between the shear modulus of the resonant layer and half-space. Hence, for $n = 0$ and $n = 1$, we can obtain the fundamental and first surface Love modes, respectively. We remark that for a vanishing resonating mass ($m_r = 0$) or equivalently $\alpha = 0$, we will have $\beta_{eff}(\omega) = \beta_1$. Therefore, Eq. (18) recovers the classical Love wave dispersion relation.

We can determine the cut-on frequency of the fundamental mode by setting $n = 0$ and assuming that the phase velocity of the propagating Love wave matches the shear wave velocity of half-space ($c = \beta_2$). After substituting these values in Eq. (18), we can then derive the angular cut-on frequency of the fundamental Love mode as:

$$w_{c,0} = \pm\omega_r\sqrt{1 - \frac{\alpha\beta_2{}^2}{(\beta_1{}^2 - \beta_2{}^2)}}. \tag{19}$$

3.3. Derivation of displacement components

The displacement formulations of Eq. (10) can be updated after substituting $A_1 = A_2$ and $A_4 = 0$ as:

$$v_1(x,z,t) = A_1\big(e^{iks_1(\omega)z} + e^{-iks_1(\omega)z}\big), \quad v_2(x,z,t) = A_3 e^{-iks_2{}^*z}, \tag{20}$$

By enforcing the continuity of displacements at the interface between the resonant layer and half-space $v_1(x,H) = v_2(x,H)$, we can obtain the relationship between the wave amplitudes as follows:

$$A_1 = \frac{e^{-kH\sqrt{1-\left(\frac{\omega}{k\beta_2}\right)^2}}}{2\cos\left(kH\sqrt{1-\left(\frac{\omega}{k\beta_{eff}(\omega)}\right)^2}\right)}A_3. \quad (21)$$

The displacement field of the Love waves and the mode shapes can be calculated using Eq. (21).

3. Numerical case study: Design of a thick locally resonant barrier for seismic Love waves

We exploit the analytically derived dispersion relation to predict the dispersive properties of seismic Love waves interacting with a meter-size thick resonant wave barrier. The mechanical parameters for the barrier and bilayer soil in a specific geophysical scenario are provided in Table 1.

Table 1. Design parameters of a thick locally resonant barrier for seismic Love waves.

Symbol	Definition	Value
β_1	Shear bulk wave speed in layer	$300\ [m/s]$
ρ_1	The mass density of the layer	$1500\ [kg/m^3]$
H	Height of layer 1	$10\ [m]$
β_2	Shear bulk wave speed of half-space	$1000\ [m/s]$
ρ_2	The mass density of half-space	$2000\ [kg/m^3]$
f_r	The resonant frequency of the resonator	$5\ [Hz]$
L	The influence length of the resonator	$1\ [m]$
α	The ratio between the mass density of the resonator and host material (soil layer 1)	$0.5\ [-]$

From Table 1, the quantities of $\mu^* = 0.067\ [-]$ and $\rho_r = \alpha\rho_1 = 750\ [kg/m^3]$ are calculated as the normalized shear modulus ratio and the mass density of the resonators, respectively.

3.1. Numerical results of dispersion analysis

The numerical investigation starts by computing the effective frequency-dependent properties of the resonant layer, utilizing the data from Table 1. Figure 2(a) presents the normalized effective mass density of the homogenized layer obtained from Eq. (1). This figure illustrates the generation of a low-frequency bulk bandgap within the frequency range of $f_{BG,bulk} = \left[f_r, f_r\sqrt{1+\alpha}\right] = [5,6.12]$ [Hz] due to the local resonance effect of the embedded resonators. In this frequency range, the effective mass density assumes negative values. The presence of the bandgap results in splitting the mass density curve into two branches with opposite phase values. We remark that as $\omega \to \infty$ (or equivalently $f \to \infty$), the effective mass density converges to $\rho_{eff} = \rho_1$, while for $f = 0$, it equals ρ_{st}.

As a result, the propagation of bulk shear waves is impeded within the bandgap frequency range, as demonstrated in Figure. 2(b), which displays the real part of the bulk wave solutions. In this case, when $f \to \infty$, the effective shear velocity is $\beta_{eff} = \beta_1$, and at frequency value equals zero, $\beta_{eff} = \sqrt{\mu_1/\rho_{st}}$.

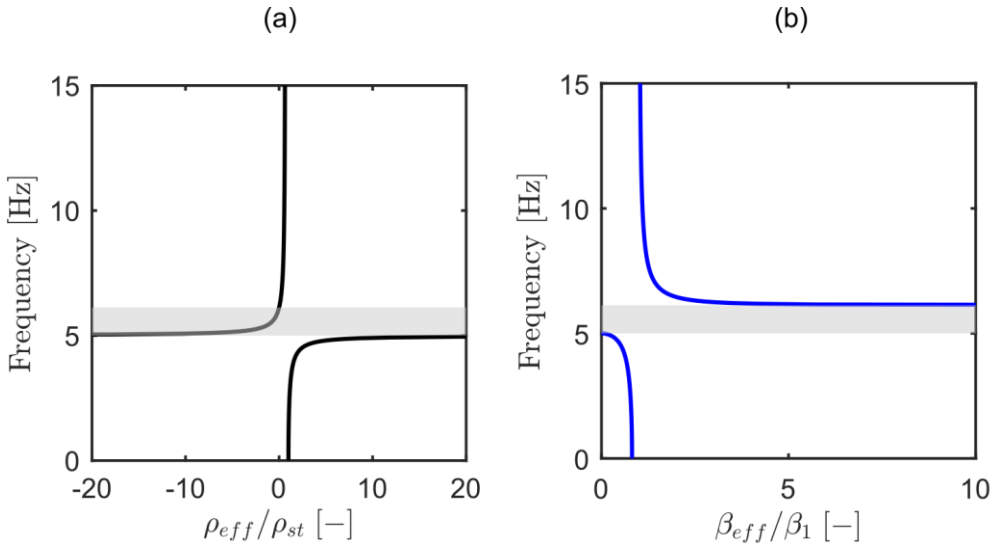

Figure 2. Effective parameters of the resonant layer. (a) Effective mass density. (b) Effective velocities of propagating bulk waves. Highlighted areas indicate the frequency bandgap.

We solved the dispersion relation represented by Eq. (18) using the Newton–Raphson root-finding algorithm. The numerical solution is obtained by utilizing the effective properties of the homogenized layer and the mechanical properties of the non-resonant half-space given in Table 1 and by sweeping the wavenumber k within the range $k = [0, k_{max}]$, where $k_{max} = \pi/L = 3.14$ [rad/m] (Palermo and Marzani 2018). The resulting dispersion relation is presented in Figure 3(a) with continuous red lines covering the frequency range of $f = [0{,}15]$ [Hz] and wavenumber in the range $k = [0{,}0.4]$ [rad/m]. These results are then compared to the classical Love wave dispersion relation (i.e., no embedded resonators), marked by dashed red lines.

In Figure 3(a), the sound cone area, where only bulk modes can propagate, is delineated by the shear bulk speed of the half-space. For the resonant layer case, the dynamic interaction of the embedded resonators and seismic Love waves results in an avoided crossing behavior between the two diverging branches of the fundamental Love mode, occurring around the collective resonant frequency of the resonators. This phenomenon is a consequence of the strong coupling of soil and resonators at resonance, which leads to the formation of a low-frequency bandgap. The lower boundary of this bandgap coincides with the resonant frequency of the resonators (f_r), while the upper boundary is the point at which the shear velocity of the half-space crosses the upper branch of the fundamental Love mode, $f_{c,0} = w_{c,0}/(2\pi) = f_r\sqrt{1 - \alpha{\beta_2}^2/({\beta_1}^2 - {\beta_2}^2)}$. It can be concluded that the propagation of seismic Love waves is effectively filtered out within the bandgap frequency range, $f_{BG,LW} = [f_r, f_{c,0}] = [5{,}6.22]$ [Hz]. It is important to note that the bandgap frequency range of Love waves is slightly wider than the bulk waves bandgap ($f_{BG,LW} > f_{BG,Bulk}$) shown in Figure 2(b). This phenomenon is due to the unique characteristics of surface waves that result in a more intricate interaction with sub-wavelength resonators, such as increased reflection.

Figure 3(b) provides a comparison of the mode shapes of the fundamental Love mode interacting with the homogenized resonant layer (continuous red line) as obtained from Eq. (20) and an isotropic layer (dashed line). This comparison is made for two frequency values indicated by red dots in the dispersion curve of Figure 3(a). The mode shapes are normalized with respect to the maximum displacement value. The results clearly demonstrate that the introduction of resonators substantially impacts the mode shape of Love waves. Specifically, for frequency values close to the resonant frequency (i.e., $f = 4.8$ [Hz]), the fundamental Love mode exhibits a high degree of confinement to the soil surface, confirming the strong dynamic coupling between the resonators and the soil at resonance.

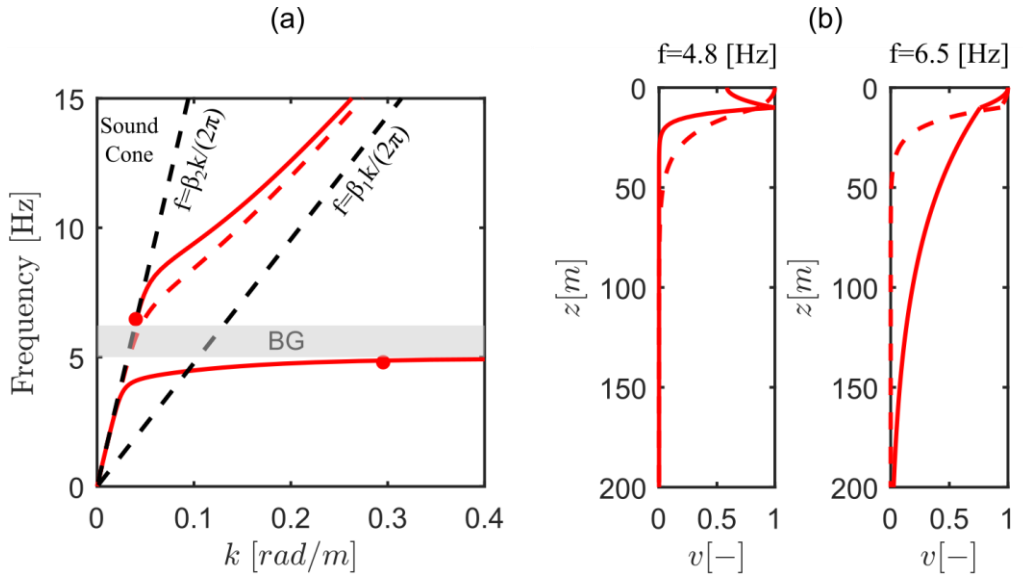

Figure 3. (a) Dispersion relation of resonant layer over a rigid half-space (continuous red lines) superimposed to the classical Love waves dispersion relation in bilayer soil (dashed red line). (b) Mode shapes of Love waves for frequency values of 4.8 and 6.5 [Hz].

3.2. Parametric study of design parameters

Our numerical investigation focuses on understanding how the design parameters of the resonators influence the dispersive characteristics of seismic Love waves. Specifically, we aim to extend the bandgap frequency range to achieve more effective attenuation of seismic Love waves. To this end, we analyze the dispersion relation for two resonant frequencies of the resonators: $f_r = 5$ [Hz] (the reference case shown in Figure 3) and $f_r = 8$ [Hz], denoted by continuous red and green lines, respectively. Our observations reveal that increasing the resonant frequency of the resonators generates a broader bandgap frequency range while preserving the overall dynamic behavior of the barrier-soil system. However, this extension comes with the cost of shifting the operating frequency of the resonators towards higher frequency ranges. This phenomenon aligns with findings in the interaction of seismic Rayleigh waves with thin metasurfaces. In Figure 4(b), we illustrate the bandgap frequency range variation due to the modifications of the resonant frequency. Both the lower and upper edges of the bandgap exhibit linear increases with increasing values of f_r. The red and green lines mark the lower and upper bounds of the bandgaps for the two case studies whose dispersion curves are shown in Figure 4(a).

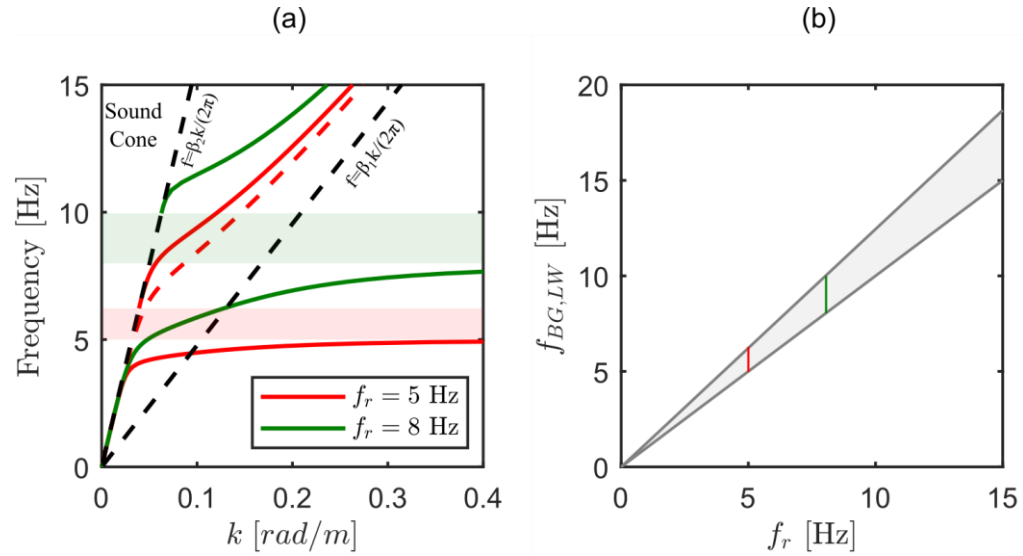

Figure 4. (a) Dispersion relation of seismic Love wave interacting with two resonant layers made of resonators with resonant frequencies of 5 [Hz] and 8 [Hz]. Highlighted areas show the bandgap regions. (b) Bandgap evolution for varying resonant frequency of the embedded resonators.

Next, we investigate the influence of the mass density ratio between the mechanical resonator and host material (soil layer 1) on the extension of the bandgap frequency range. To this end, we consider two values of $\alpha = 0.5$ (the reference case in Figure 3) and $\alpha = 0.9$. The dispersion relation of these two cases is presented in Figure 5(a) with continuous red and yellow lines, respectively. As we increase the value of α, the overall dispersive behavior of seismic Love waves interacting with a resonant layer remains consistent. However, the width of the bandgap frequency range expands. In Figure 5(b), we illustrate the variation in the bandgap frequency range with changes in α values. It is noteworthy that while the lower edge of the bandgap remains constant, the upper edge increases as α values rise since $f_{c,0}$ is a function of the square root of α. The mass density ratio plays a fundamental role in governing the dynamic interaction between the resonators and the soil layer, controlling the stress exchange mechanism. For example, when there are no resonators ($\alpha = 0$), a bandgap does not emerge. However, as the relative inertia between the resonator and the soil becomes more significant, corresponding to higher values of α, a more considerable amount of stress will be exchanged, generating a relatively broader bandgap frequency range.

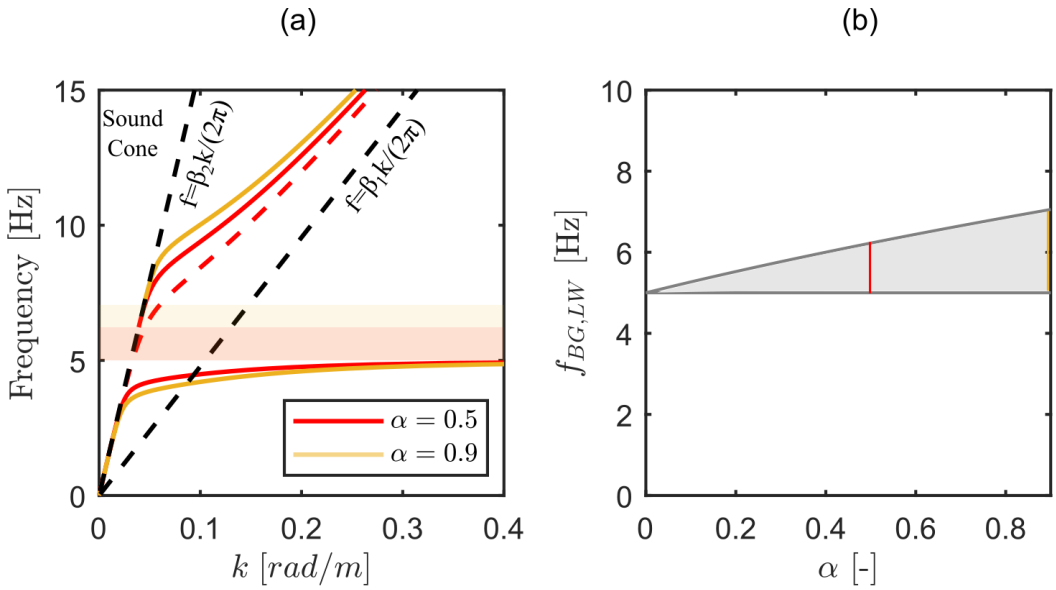

Figure 5. (a) Seismic Love wave dispersion relation with varying mass density ratio (α). Highlighted areas show the bandgap regions. (b) Bandgap evolution with changing α.

4. Conclusions

We studied the dynamic interaction between seismic Love waves and a resonant layer attached to a stiffer half-space. This resonant layer comprises sub-wavelength mechanical resonators embedded within the soil. To determine the effective mechanical properties of an equivalent homogenized layer, we applied a homogenization technique suitable for the long-wavelength approximation. These effective parameters were then utilized to derive an original dispersion relation, following the conventional approach for deriving dispersion relations of Love waves in a bilayer media. We employed a numerical root-finding method to solve this dispersion relation, examining the dispersive characteristics of the system within a real geophysical context.

From the dispersion analysis, we noted that the dynamic interaction between seismic Love waves and the resonant layer gives rise to a narrow and low-frequency bandgap around the collective resonant frequency of the resonators. More importantly, this dispersive behavior differs from the Love wave interaction with elastic metasurfaces, where the resonators are attached to the soil surface, and the bandgap frequency is absent.

We conducted a parametric analysis of the design parameters of mechanical oscillators to explore their impact on expanding the bandgap frequency range. We observed that increasing the resonant frequency results in an extension of the bandgap frequency range, albeit at the cost of shifting the operating frequency to higher values. Given our focus on the low-frequency range characteristic of seismic surface waves, we investigated the potential for widening the bandgap without altering the resonant frequency. Our findings indicate that by increasing the relative inertia of the resonators with respect to the soil's mass density, or, in other words,

increasing the α values, the bandgap frequency range can be broadened while preserving the overall dynamic behavior. It is worth noting that the mass density ratio governs the dynamic interaction between the resonator and the soil, thereby regulating the transfer of stresses between them.

The outcomes of this work provide new insights for the analysis and design of locally resonant metamaterial devices aimed at controlling and manipulating the propagation of surface waves across various frequency ranges. Such applications hold promise in diverse engineering disciplines, including earthquake, acoustics, road and railway traffic, and geotechnics.

Acknowledgments

F.Z. acknowledges funding from the Italian Ministry of Education, Universities, and Research (MIUR) for the "ELeMEnT" project under grant agreement SOE0000157.

5. References

Brûlé, S., E. H. Javelaud, S. Enoch and S. Guenneau (2014). "Experiments on Seismic Metamaterials: Molding Surface Waves." *Physical Review Letters* 112(13): 133901.

Brûlé, S., B. Ungureanu, Y. Achaoui, A. Diatta, R. Aznavourian, T. Antonakakis, R. Craster, S. Enoch and S. Guenneau (2017). "Metamaterial-like transformed urbanism." *Innovative Infrastructure Solutions* 2(1): 20.

Colombi, A., V. Ageeva, R. J. Smith, A. Clare, R. Patel, M. Clark, D. Colquitt, P. Roux, S. Guenneau and R. V. Craster (2017). "Enhanced sensing and conversion of ultrasonic Rayleigh waves by elastic metasurfaces." *Scientific Reports* 7(1): 6750.

Colombi, A., P. Roux, S. Guenneau, P. Gueguen and R. V. Craster (2016). "Forests as a natural seismic metamaterial: Rayleigh wave bandgaps induced by local resonances." *Scientific Reports* 6(1): 19238.

Colquitt, D. J., A. Colombi, R. V. Craster, P. Roux and S. R. L. Guenneau (2017). "Seismic metasurfaces: Sub-wavelength resonators and Rayleigh wave interaction." *Journal of the Mechanics and Physics of Solids* 99: 379-393.

Huang, H. H., C. T. Sun and G. L. Huang (2009). "On the negative effective mass density in acoustic metamaterials." *International Journal of Engineering Science* 47(4): 610-617.

Jiao, P., J. Mueller, J. R. Raney, X. Zheng and A. H. Alavi (2023). "Mechanical metamaterials and beyond." *Nature Communications* 14(1): 6004.

Krodel, S., N. Thome and C. Daraio (2015). "Wide bandgap seismic metastructures." *Extreme Mechanics Letters* 4: 111-117.

Love, A. E. H. (1911). Some Problems of Geodynamics: Being an Essay to which the Adams Prize in the University of Cambridge was Adjudged in 1911, University Press.

Maurel, A., J.-J. Marigo, K. Pham and S. Guenneau (2018). "Conversion of Love waves in a forest of trees." *Physical Review B* 98(13): 134311.

Miniaci, M., A. Krushynska, F. Bosia and N. M. Pugno (2016). "Large scale mechanical metamaterials as seismic shields." *New Journal of Physics* 18(8): 083041.

Mu, D., H. Shu, L. Zhao and S. An (2020). "A Review of Research on Seismic Metamaterials." *Advanced Engineering Materials* 22(4).

Palermo, A., S. Krödel, A. Marzani and C. Daraio (2016). "Engineered metabarrier as shield from seismic surface waves." *Scientific Reports* 6(1): 39356.

Palermo, A. and A. Marzani (2018). "Control of Love waves by resonant metasurfaces." *Scientific Reports* 8(1): 7234.

Pillarisetti, L. S. S., C. J. Lissenden and P. Shokouhi (2022). "Control of Rayleigh wave propagation through imposing Mindlin boundary conditions on the surface." *Journal of Sound and Vibration* 530: 116931.

Pu, X., A. Palermo, Z. Cheng, Z. Shi and A. Marzani (2020). "Seismic metasurfaces on porous layered media: Surface resonators and fluid-solid interaction effects on the propagation of Rayleigh waves." *International Journal of Engineering Science* 154: 103347.

Pu, X. and Z. Shi (2018). "Surface-wave attenuation by periodic pile barriers in layered soils." *Construction and Building Materials* 180: 177-187.

Xu, Y., Z. Cao, K. Cui, Y. Cai and X. Pu (2023). "Tunable metasurfaces for seismic Love wave manipulation: A theoretical study." *International Journal of Mechanical Sciences* 251: 108327.

Zaccherini, R., A. Palermo, A. Marzani, A. Colombi, V. Dertimanis and E. Chatzi (2020). "Mitigation of Rayleigh-like waves in granular media via multi-layer resonant metabarriers." *Applied Physics Letters* 117(25).

Zeighami, F., A. Palermo and A. Marzani (2019). "Inertial amplified resonators for tunable metasurfaces." *Meccanica* 54(13): 2053-2065.

Zeighami, F., A. Palermo and A. Marzani (2021). "Rayleigh waves in locally resonant metamaterials." *International Journal of Mechanical Sciences* 195: 106250.

Zeighami, F., L. Sandoval, A. Guadagnini and V. Di Federico (2023). "Uncertainty quantification and global sensitivity analysis of seismic metabarriers." *Engineering Structures* 277.